Transconductance quantization in a topological Josephson tunnel junction circuit

L. Peyruchat,[1] J. Griesmar,[1,*] J.-D. Pillet,[1,2] and Ç. Ö. Girit[1,†]

[1]*Flux Quantum Lab (Φ_0), JEIP, USR 3573 CNRS, Collège de France, PSL University, 11, place Marcelin Berthelot, 75231 Paris Cedex 05, France*

[2]*LSI, CEA/DRF/IRAMIS, Ecole Polytechnique, CNRS, Institut Polytechnique de Paris, F-91128 Palaiseau, France*

(Received 25 September 2020; revised 1 February 2021; accepted 2 February 2021; published 29 March 2021)

Superconducting circuits incorporating Josephson tunnel junctions are widely used for fundamental research as well as for applications in fields such as quantum information and magnetometry. The quantum coherent nature of Josephson junctions makes them especially suitable for metrology applications. Josephson junctions suffice to form two sides of the quantum metrology triangle, relating frequency to either voltage or current, but not its base, which directly links voltage to current. We propose a five Josephson tunnel junction circuit in which simultaneous pumping of flux and charge results in quantized transconductance in units $4e^2/h = 2e/\Phi_0$, the ratio between the Cooper pair charge and the flux quantum. The Josephson quantized Hall conductance device (JHD) is explained in terms of intertwined Cooper pair pumps driven by the AC Josephson effect. We describe an experimental implementation of the device and discuss the optimal configuration of external parameters and possible sources of error. The JHD has a rich topological structure and demonstrates that Josephson tunnel junctions are universal, capable of interrelating frequency, voltage, and current via fundamental constants.

DOI: 10.1103/PhysRevResearch.3.013289

I. INTRODUCTION

Among quantum coherent electronic components, the most prominent are Josephson junctions and quantum Hall systems. The physics describing electrons in both systems is rich and has yielded numerous applications in sensing, quantum information, and metrology. Josephson junctions, due to their nonlinearity, serve as the qubit building blocks of superconducting quantum computers [1] and sensitive magnetometers [2]. In metrology, this nonlinearity, the Josephson relation, allows employing such junctions to define the voltage standard, with an accuracy much better than parts per billion [3,4]. Such junctions can also be used to obtain quantized currents, albeit with less accuracy than the Josephson voltage standard [5,6]. Both metrological standards work by pumping Josephson junction circuits at a precise frequency f, obtaining either the quantized voltage $V = n\Phi_0 f$ or the quantized current $I = 2enf$, where n is an integer and the fundamental constants are the magnetic flux quantum $\Phi_0 = h/2e$ and electron charge e. In principle, two sides of the quantum metrology triangle [7] (Fig. 1), which link frequency, voltage, and current, can be completed using Josephson junctions only. Given that the two noncommuting observables in a quantum circuit are number (charge) $\hat{N}$ and phase (flux) $\hat{\delta}$, it is not surprising that current and voltage, their respective time derivatives, can be quantized and used for metrology.

What is surprising, however, is that it has not been possible to use Josephson tunnel junctions to close the base of the metrology triangle, directly relating voltage to current. Transconductance quantization is defined as a transverse or Hall voltage V_Y, which is related to a longitudinal current I_X by a resistance which depends only on fundamental constants. Typical experimental implementations of transconductance quantization rely on semiconducting systems such as two-dimensional (2D) electron gases in which there is a robust quantum Hall effect upon application of relatively large magnetic fields [8]. With recent graphene-based standards, it is possible to reduce the required magnetic field to several tesla and increase the operating temperature up to 10 k [9]. In these semiconducting systems, the relevant resistance is the von Klitzing constant $R_K = h/e^2$, and is quantized on the order of parts per billion. For superconducting systems, the constant of proportionality between voltage and current would be the superconducting resistance quantum $R_Q = h/4e^2$, which is more suggestively written as the ratio of the flux quantum to the Cooper pair charge $R_Q = \Phi_0/2e$. This evocative relationship motivates the search for a Josephson junction circuit in which flux quanta and charge quanta are pumped simultaneously, producing a quantized resistance.

A circuit incorporating a Josephson tunnel junction and an LC resonator was proposed to quantize transconductance, but requires an impractical quantum phase-slip element [10]. Nontrivial topology was identified in the Andreev bound-state spectrum of multiterminal superconducting devices [11–13] and it was shown that such systems could also exhibit a quantized Hall conductance [14–17]. Although these multiterminal weak link systems have motivated several experiments [18–20], topological effects depend on the existence of highly transmitting microscopic Andreev states and device synthesis is challenging. We propose a circuit containing

*Present address: Institut Quantique et Département GEGI, Université de Sherbrooke, Sherbrooke, QC, Canada.

†caglar.girit@college-de-france.fr.

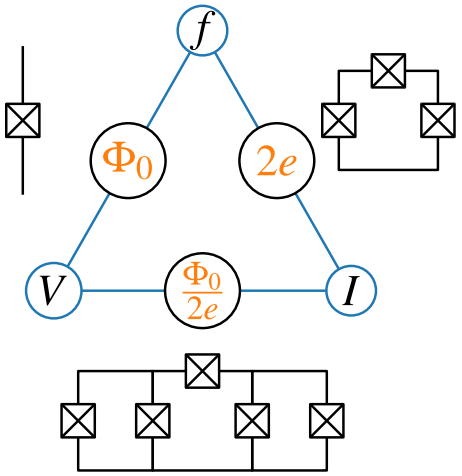

FIG. 1. Completing the metrology triangle with only Josephson tunnel junctions. Circuits containing Josephson tunnel junctions (black crosses) can be used to form the metrology triangle relating voltage V, current I, and a pump signal at frequency f via the fundamental constants $2e$, $\Phi_0 = h/2e$, and their ratio $R_Q = \Phi_0/2e = h/4e^2$. In the AC Josephson effect (upper left), a microwave drive pumps flux quanta across a Josephson junction at a rate f yielding the quantized voltage $V = \Phi_0 f$. In a Cooper pair pump (upper right), the microwave drive pumps Cooper pairs (charge $2e$) at a rate f yielding a quantized current $I = 2ef$. A circuit with five Josephson junctions, the Josephson quantized Hall conductance device (bottom), combines both Cooper pair and flux pumping to yield a quantized Hall voltage $V_Y = R_Q I_X$ as in the quantum Hall effect.

only five Josephson tunnel junctions, the Josephson quantized Hall conductance device (JHD), which quantizes V_Y at sub-tesla magnetic fields while requiring only conventional fabrication techniques. Not only is the Hamiltonian for our device completely different from that of Andreev-based systems, engineering the circuit is relatively easy as the required technology is mature, there are less constraints on the circuit dimensions, no junction requires more than two terminals, and the junction transparencies may be small.

II. FLUX AND CHARGE QUANTIZATION

The upper sides of the quantum metrology triangle (Fig. 1) correspond to flux and charge pumping, processes which occur simultaneously in the JHD. Flux pumping can be understood by considering the phase evolution in the AC Josephson effect. A single Josephson junction [Fig. 1 (upper left)] biased at a voltage V_J will have a superconducting phase δ which evolves linearly in time at the Josephson frequency $\omega_J = \dot{\delta} = V_J/\varphi_0$, where $\varphi_0 = \Phi_0/2\pi$ is the reduced flux quantum. A 2π change in δ corresponds to pumping one fluxoid and occurs at a rate $f_J = \omega_J/2\pi$. In Josephson voltage standards, a microwave signal at frequency f is used to synchronize fluxoid pumping so that $f_J = nf$ and the voltage V_J is determined with a precision limited only by the microwave reference clock and not by thermal noise in the DC voltage supply [3]. The topological nature of fluxoid quantization as well as charge quantization and the quantum Hall effect is highlighted by Thouless [21,22].

To relate frequency to current [Fig. 1 (upper right)], the relevant superconducting circuit is the Cooper pair pump (CPP) [Fig. 2(a)], consisting of three Josephson tunnel junctions (red boxed crosses) in series, forming two superconducting islands with canonical quantum variables $\hat{n}_{1,2}$ and $\hat{\delta}_{1,2}$ [24,25]. For simplicity, we consider identical junctions. We define the charging energy as $E_C = (2e)^2/2C$, where C is the junction capacitance. Charge offsets n_{g1}, n_{g2} have DC components n^0_{g1}, n^0_{g2} determined by static gate biases (not shown) and AC components n^1_{g1}, n^1_{g2} determined by a microwave pump of amplitude V^1_g and radial frequency ω. A θ-phase shifter (green) allows dephasing the oscillating parts on each island.

Ignoring the Josephson part of the Hamiltonian, the CPP has stable charge states on hexagonal plaquettes shown in the bottom plane of Fig. 2(b), delineated by gray lines denoting charge degeneracies. The AC modulation of both gate voltages around a plaquette vertex, a point of triple degeneracy, can be used to cycle between charge states and drive exactly one Cooper pair across the device per cycle. The Josephson coupling terms hybridize the charge states with strength E_J, the Josephson energy. The characteristic energy scale is now $\hbar\omega_p = \sqrt{2E_J E_C}$, where $\omega_p = 1/\sqrt{L_J C}$ is the plasma frequency, and the dimensionless impedance $\alpha = Z_J/R_Q = 1/2\pi\sqrt{2E_C/E_J}$ characterizes the ratio between charging energy and Josephson energy. The Josephson inductance is defined by $E_J = \varphi_0^2/L_J$ and is related to the critical current $I_0 = \varphi_0/L_J$. The reduced magnetic flux $\varphi_X = B_X A/\varphi_0$, determined by an external magnetic field B_X threading the three-junction loop of area A, can be used to change the Josephson coupling between islands. Nontrivial topological effects can arise when the energy spectrum has degeneracies at certain points in the parameter space. At $\varphi_X = \pi$ the Josephson coupling is effectively turned off, so there are two degeneracies, Fig. 2(c), and modulating the gate voltages pumps exactly one Cooper pair each time the trajectory winds around a degeneracy. But for any other value of φ_X, the degeneracies are lifted and a gate voltage cycle no longer results in quantized charge transfer.

This error in pumped charge can in principle be averaged out by covering a closed surface around the degeneracy with a helical trajectory as shown in Fig. 2(b) [25,26]. The helix maps out a cylinderlike surface centered at charge offset n^0_{g1}, n^0_{g2}. The radial profile is determined by the AC amplitude V^1_g and phase shift θ whereas the upward velocity is given by $\dot{\varphi}_X$. Taking into account the 2π periodicity of φ_X, the cylinder shown in Fig. 2(b) ($\theta = \pi/2$) is actually a torus T^2 in parameter space. The pumped charge is proportional to the integral of the Berry curvature over T^2 which is equal to 2π times the Chern number $C(T^2)$. The average current across the CPP is then given by $I = 2efC(T^2)$, where the microwave pump frequency $f = \omega/2\pi$ is also the winding rate in the n_{g1}, n_{g2} plane. It is interesting to note that this current does not depend on the value nor on the sign of $\dot{\varphi}_X$ as long as $\dot{\varphi}_X \neq 0$ and is incommensurate with ω [26]. The phase ramp $\dot{\varphi}_X$ can be applied by inductively coupling to the CPP loop [26] or inserting a voltage source [24].

Current quantization is insensitive to small variations in junction critical currents and capacitances as the resulting modifications to E_{Ji}, E_{Ci} only move the degeneracies in the

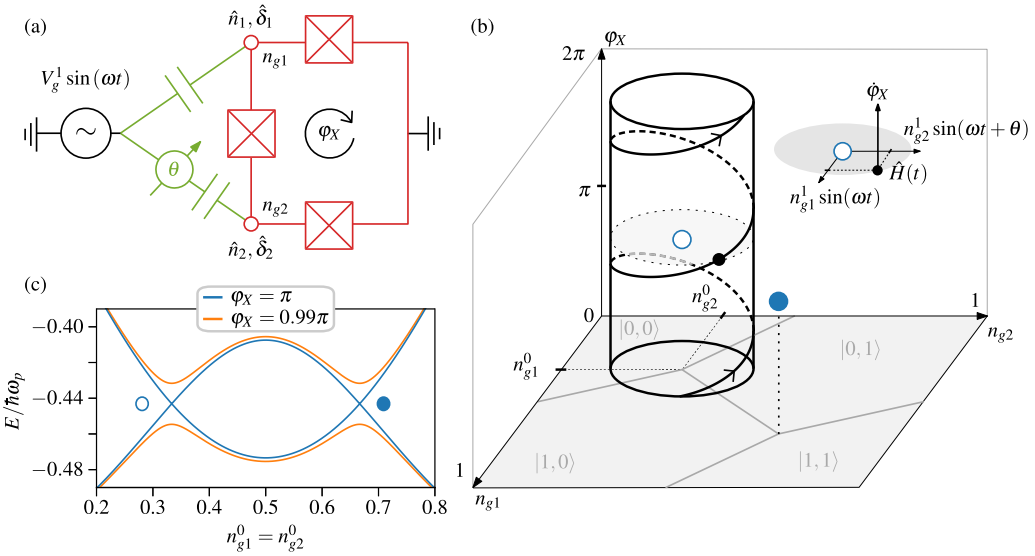

FIG. 2. Topological Cooper pair pumping. (a) The Cooper pair pump (CPP) consists of three Josephson tunnel junctions in series (red boxed crosses), forming two superconducting islands with canonical quantum variables $\hat{n}_{1,2}$ and $\hat{\delta}_{1,2}$. Gate voltages applied via a microwave pump and additional DC sources (not shown) determine the charge offsets n_{g1}, n_{g2} on the islands. An external magnetic field tunes the reduced magnetic flux φ_X. (b) The three periodic parameters n_{g1}, n_{g2} and φ_X form a parameter space analogous to a three-dimensional (3D) Brillouin zone [23]. Degeneracies in the spectrum are indicated by blue dots on the $\varphi_X = \pi$ plane and are associated with topological charges ± 1. The current flowing through the CPP, $I = 2ef$, is quantized on a cyclic trajectory in parameter space which encloses a degeneracy ($f = \omega/2\pi$). (c) The two lowest-energy bands of the circuit are plotted for equal DC charge offset $n_{g1}^0 = n_{g2}^0$ and $E_J/E_C = 1$. There are two degeneracies in the spectrum for $\varphi_X = \pi$ (blue) and none for other values (e.g., $\varphi_X = 0.99\pi$, red). Energy is plotted in units of plasma frequency $\hbar\omega_p = \sqrt{2E_J E_C}$ and all junctions are identical.

$\varphi_X = \pi$ plane but do not destroy them. The first experiments employing topological pumping of CPPs had low currents and significant error [24], but optimization can mitigate factors such as nonadiabaticity and supercurrent leakage [26], resulting in improved performance [25]. Significant amelioration is still necessary before they can serve as current standards for metrology [6], and larger currents are obtained by combining the conventional QHE and Josephson voltage standard [27].

III. TRANSCONDUCTANCE QUANTIZATION

A circuit exploiting the AC Josephson effect to replace both microwave pumps of the CPP by voltage-biased Josephson junctions allows combining flux and charge pumping to directly link voltage and current via a quantized conductance. The key point is that the microwave pump frequency f can be associated with a Josephson frequency $\omega_J = 2\pi f$ and the pump amplitude V_g^1 with the critical current. The five-junction circuit shown in Fig. 3 is one realization of a Josephson quantized Hall conductance device which closely resembles the CPP circuit in Fig. 2(a). Due to the Josephson effects, the green Josephson junctions convert the input DC voltage V_L into oscillating currents at frequency ω_{JL} and amplitude proportional to their critical currents I_0. We assume that the critical currents of the other junctions (red) are large enough such that the DC voltage V_L drops only across the green junctions. Although this assumption is not essential for transconductance quantization, it helps establish the analogy with the CPP microwave driving circuit in Fig. 2(a). The oscillating Josephson currents result in oscillating voltages V_1 and V_2 which drive the charge nodes of the CPP formed by the three red junctions on the right. Due to the topologically nontrivial nature of the CPP spectrum, current quantization holds for a large range of amplitudes for V_1, V_2 determined by the junction impedances $Z_{Ji} = \sqrt{L_{Ji}/C_{Ji}}$. The phase difference $\gamma(\varphi_B)$ between the two leftmost green junctions can be

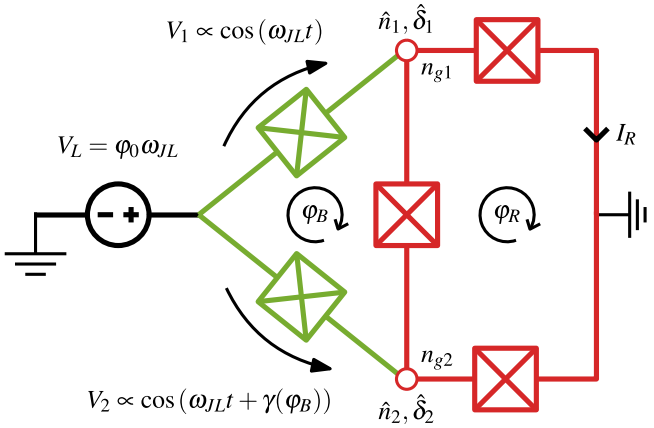

FIG. 3. Driving a Cooper pair pump with the AC Josephson effect. The constant voltage bias V_L is converted by the green Josephson junctions (boxed crosses) into oscillating currents $I_L \approx I_0 \sin(\omega_{JL} t)$, where I_0 is their critical current. These currents generate oscillating voltages V_1 and V_2 at the charge nodes of a Cooper pair pump (CPP) formed by the three red junctions. The reduced magnetic flux $\varphi_B = \Phi_B/\varphi_0$ threading the central loop introduces a phase offset $\gamma(\varphi_B)$ between these oscillating voltages ($\varphi_B = \Phi_0/2\pi$). An additional ramp of the flux φ_R results in a quantized current $I_R = 2e\omega_{JL}/2\pi = V_L 4e^2/h = V_L/R_Q$ flowing through the red CPP.

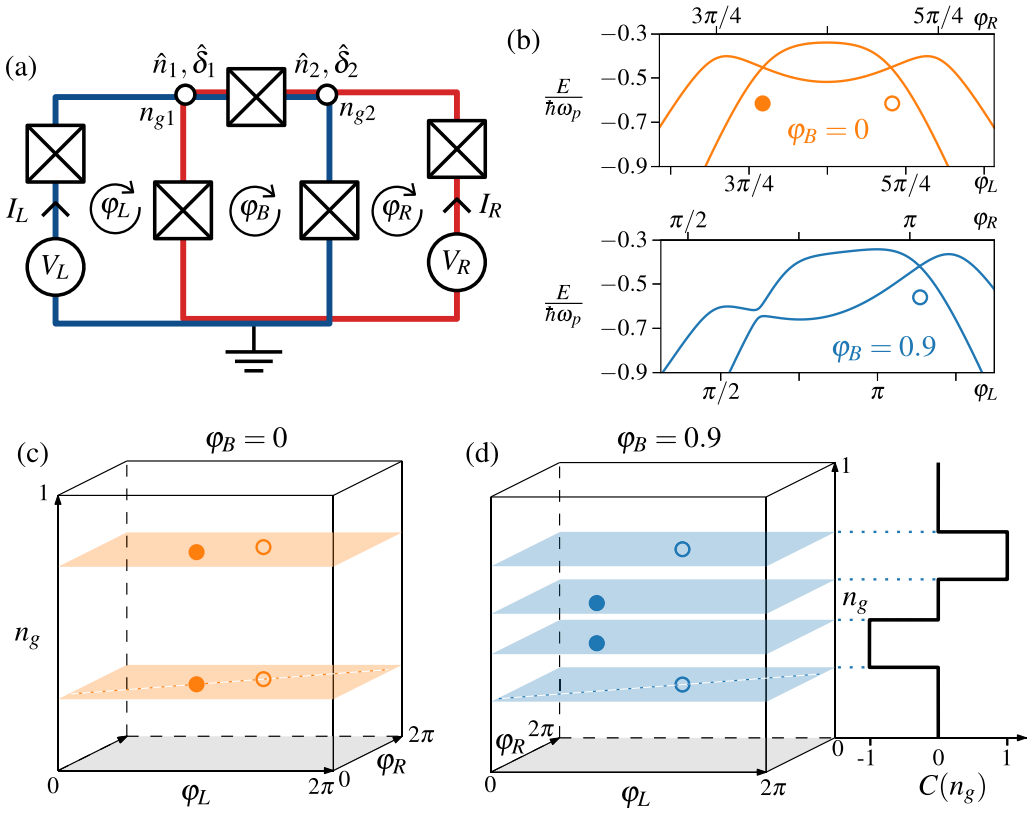

FIG. 4. Topological properties of the Josephson quantized Hall conductance device. (a) The circuit consists of five Josephson tunnel junctions (boxed crosses) forming two superconducting islands (circled) and three loops. Gate voltages applied to each island (not shown) determine the global offset charge n_g and along with the loop fluxes $\varphi_{L,B,R}$ tune the energy spectrum of the system. The constant voltage sources V_L and V_R allow linearly ramping φ_L and φ_R and supply currents $I_{L,R}$. (b) The two lowest-energy bands containing degeneracies are plotted for $n_g \approx 0.25$ along cuts indicated in the bottom φ_L, φ_R planes of (c) and (d) (dashed lines). As φ_B is tuned away from zero (top, orange) one of the degeneracies is lifted (bottom, blue). Degeneracies with topological charge $+1$ (-1) are indicated by filled (unfilled) circles. (c) The positions of degeneracies are indicated in the 3D parameter space φ_L, φ_R, n_g. For $\varphi_B = 0$ pairs of degeneracies with opposite signs are located on planes of constant n_g, resulting in a Chern number of zero. (d) For nonzero φ_B the $+1$ degeneracies (filled circles) split off the planes in (c) and shift toward $n_g = 0.5$. The Chern number, plotted on the right, is ± 1 for n_g lying between two opposite charge degeneracies and zero elsewhere. Details of the Hamiltonian, parameters, and positions of the degeneracies are provided in Fig. 6

tuned with the reduced magnetic flux φ_B, with the function γ accounting for the current-phase dependence of the three-junction loop [28,29]. Compared to the microwave gate drives of the CPP of Fig. 1(a), the amplitudes $V_{1,2}$ correspond to V_g^1 and $\gamma(\varphi_B)$ to the phase shift θ. With additional DC gate biasing to obtain the proper charge offsets on the superconducting islands and a series voltage source V_R in the red CPP loop to ramp φ_R, we completely reproduce the pumping protocol of Fig. 2. The current pumped in the right CPP is quantized and given by $I_R = 2e\omega_{JL}/2\pi = V_L 4e^2/h = V_L/R_Q$. Although the JHD shown in Fig. 3 is conceptually closest to the CPP of Fig. 2(a), the symmetric circuit of Fig. 4(a) also quantizes transconductance and more clearly demonstrates that there are actually two intertwined Cooper pair pumps, indicated in blue and red. One JHD circuit can be transformed into another by shifting the sources and rotating the branches (see Appendix). In the following, we show by topological arguments that each time a flux quantum is pumped in one CPP loop of the symmetric JHD, a Cooper pair is pumped in the other CPP loop, resulting in transconductance quantization.

For the numerically computed spectra and degeneracies in Figs. 4(b)–4(d) we assume for simplicity that the charge offset on both islands is n_g. To show that symmetry is not necessary for transconductance quantization we treat the experimentally relevant situation in which the plasma frequency of all junctions is identical but not their surface areas. The full Hamiltonian, junction parameters, positions, and topological charges of the degeneracies, as well as a description of numerical methods, are provided in the Appendix.

The Josephson quantized Hall conductance device, which realizes the quantum Hall effect with only Josephson tunnel junctions, can be understood by examining the topological properties of the circuit. Transconductance quantization can be linked to the system's Hamiltonian and eigenstates via a Chern number (see Appendix). As with the degeneracies in the energy spectrum of the CPP, those of the JHD [Fig. 4(b)] are also associated with topological charges ± 1 (filled and unfilled circles, respectively). The Brillouin zone φ_L, φ_R, n_g and positions of degeneracies are shown in Figs. 4(c) and 4(d). As in the Andreev-state-based topologically nontrivial systems [14–16] to encompass a degeneracy the φ_L, φ_R plane is swept by applying constant incommensurate voltages $V_L = \varphi_0\dot{\varphi}_L$ and $V_R = \varphi_0\dot{\varphi}_R$. Unlike the multiterminal Andreev devices which have a different Hamiltonian, the JHD has charge

offset parameters n_g in addition to fluxes $\varphi_{B,L,R}$. When a plane crosses a degeneracy, the corresponding Chern number $C(n_g, \varphi_B)$ changes by the value of the topological charge. We take the convention that topological charges are added to the Chern number in the direction of increasing n_g. For $\varphi_B = 0$, shown in orange in Figs. 4(b) and 4(c), pairs of degeneracies with opposite topological charges are located on the same n_g plane and the Chern number is always zero. On the contrary, for nonzero values such as $\varphi_B = 0.9$, shown in blue in Figs. 4(b) and 4(d), single degeneracies exist in the φ_L, φ_R plane for certain values of n_g and the Chern number can be ± 1.

For a given eigenstate the associated instantaneous current through one of the loops has a contribution from the junction supercurrents, but this dynamical term averages out to zero for an adiabatic sweep of the entire φ_L, φ_R plane. The second contribution comes from the Berry curvature which when integrated over this plane is proportional to the Chern number. This geometric contribution gives rise to DC currents I_L (I_R) which are quantized [14,30]

$$I_{L,R}(n_g, \varphi_B) = \frac{4e^2}{h} C(n_g, \varphi_B) V_{R,L}, \tag{1}$$

and depend on the voltage V_R (V_L) applied to the opposite loop (see Appendix). Referring to the circuit Fig. 4(a), this transconductance is interpreted as two Cooper pair pumps (red and blue loops) acting as AC Josephson drives for one another such that the pumped current through one depends on the Josephson frequency of the other. The current circulating in the middle loop threaded by φ_B, unlike I_L and I_R, is not quantized. Although the eigenstates of the multiterminal Andreev systems are not the same as for the JHD, since Eq. (1) is independent of the basis, transconductance is quantized in both systems.

IV. DISCUSSION

The topology of the JHD and isolated CPP can be compared to understand why flux and charge are pumped in the JHD and only charge is pumped in the CPP. The cylinder of Fig. 2(b) and the plane of Figs. 4(c) and 4(d) both correspond to tori covering only one degeneracy and imply charge pumping. The CPP trajectory in the n_{g1}, n_{g2} plane does not reach the Brillouin zone boundaries, unlike the vertical component (φ_X). On the contrary, the JHD bias voltages $V_{L,R}$ result in both parameters φ_L, φ_R crossing the Brillouin zone boundary. These crossings correspond to pumping of two fluxoids in the JHD circuit loops.

The value of the Chern number $C(n_g, \varphi_B) = \pm 1$ as well as the minimum energy gap in the φ_L, φ_R plane is plotted in the phase diagram, Fig. 5, as a function of n_g and φ_B for the same junction configuration E_{Ji}, E_{Ci} as in Fig. 4. The black lines where the gap vanishes demarcate the different topological regions. The Chern number in the central and exterior trivial regions is equal to zero and its label is omitted. The relative placement of Chern numbers can be explained by general symmetry arguments for Josephson junction circuits [31]. Overall inversion symmetry of the Hamiltonian implies that the Chern number is conserved when all parameters are inverted. This results in the configuration of Fig. 5, where inverting both n_g and φ_B, and implicitly φ_L and φ_R, maintains the sign of the Chern number. Time-reversal symmetry on the other hand corresponds to inverting either all charge parameters or all flux parameters, changing the sign of the Chern number. As a result, the topologically nontrivial region has a quadrupolelike distribution which occupies a large fraction of the phase space. The size of this region will shrink as junction disorder increases, but as long as the operating point for the JHD remains in a region of nonzero Chern number, the pumped current will be quantized.

In addition to labels for the Chern number, Fig. 5 has blue and orange circles which correspond to the degeneracies of Figs. 4(b)–4(d). For a charge of a given sign (filled or unfilled circle), continuity implies that it follows the dark blue degeneracy lines as n_g and φ_B are varied. For example, the -1 charge at $n_g \approx \frac{1}{4}$; $\varphi_B = 0$ (bottom unfilled orange circle) moves horizontally to the right whereas the $+1$ charge (bottom filled orange circle) moves upward toward $n_g = \frac{1}{2}$, flanking the nontrivial region in the lower right with Chern number -1. The two $+1$ charges (filled blue circles) join at the line $n_g = 0.5$ as φ_B increases, eventually followed by the two -1 charges (unfilled blue circles) as φ_B approaches π. When all junctions are identical, the outer corners of the four non-trivial regions extend out to $n_g \approx \frac{1}{4}, \frac{3}{4}$; $\varphi_B = \pm\pi$ and the size of the central trivial region shrinks as the ratio E_J/E_C increases (Fig. 8).

Transconductance quantization only holds in the adiabatic limit, so it is important that the pump frequencies, determined by V_L and V_R, are small compared to the plasma frequency [23]. This limitation was studied in detail for Andreev multiterminal devices in which the corresponding energy scale, the superconducting gap, is several times larger [14,15]. A typical value for the plasma frequency of aluminum Josephson junctions is 20 GHz, corresponding to $\varphi_0\omega_p = 40\ \mu$V. Applied voltages must be much smaller than $\varphi_0\omega_p$ to avoid inducing Landau-Zener transitions (LZT) from the ground state to excited states. As the LZT probability scales inversely with the square of the energy gap, the JHD should be operated at values of n_g, φ_B that maximize the smallest gap along the trajectory, the φ_L, φ_R plane. From Fig. 5 this optimum is near $n_g = \frac{1}{3}$ and $\varphi_B = \pi/2$, where the minimum gap is roughly equal to $0.1\omega_p$ or 2 GHz (4 μV). For good quantization the applied voltages must be smaller than this value, resulting in pumped currents which are smaller than 150 pA.

In the case of identical junctions, the choice of the scaled junction impedance $\alpha = Z_J/R_Q$, requiring careful device design and junction fabrication, is also important to minimize noise. The parameter α is an effective fine-structure constant and is inversely proportional to the junction surface area. By making small junctions one can obtain much larger values than $\alpha_0 = Z_0/8R_Q \approx \frac{1}{137}$, where Z_0 is the vacuum impedance, greatly modifying the phase diagram of Fig. 5. Comparison is made for different values of α in Fig. 8. We find that the minimum gap is largest for $\alpha \simeq \frac{1}{2}$, allowing increased pump currents while remaining adiabatic. Optimizing the value of α for transconductance quantization is analogous to impedance matching Z_J, in this case to approximately $R_Q/2$. Although deviating from the optimum will decrease the gap, reducing α also comes at the cost of enhanced supercurrent

leakage, as noise in φ_B and n_g prevents the dynamical contribution of the current from averaging to zero during the φ_L, φ_R sweep. Other sources of error which have already been analyzed in depth for Cooper pair pumps [25,26] are the effect of the external biasing circuit, thermal population of excited states, co-tunneling, and quasiparticle poisoning. Although some proposed error mitigation techniques can be directly applied to our circuit, implementing other techniques such as shortcut-to-adiabaticity [32] would be more difficult.

Fabricating the Josephson quantized Hall conductance device, given current technology for superconducting circuits containing hundreds of Josephson tunnel junctions, is straightforward. This is in contrast to quantized Hall transconductance devices based on phase-slip or high-transparency multiterminal weak links. Using niobium, with a higher critical current density than aluminum, is desirable for increasing the plasma frequency and extending the range for adiabatic operation. Static control of loop fluxes can be accomplished with inductive coupling and charge offsets can be adjusted with local gates.

As with conventional quantum Hall resistance standards, and unlike Josephson current or voltage standards, the Josephson quantized Hall conductance device does not require an external microwave pump. Applying voltages V_L and V_R could exploit strategies from CPP experiments such as inserting small resistances into the left and right loops which are biased by external current sources [33]. A more clever strategy would directly apply a voltage difference across these two resistances. To preserve phase coherence over timescales comparable to the pump frequency, the resistances r should be small enough such that $I_0 r \ll V_{L,R}$ [34]. Although noise of the external sources should be minimized in principle, the pumped current will follow fluctuations in V_L and V_R such that the transconductance remains quantized. Measurement of the pumped currents I_L and I_R can be made by borrowing techniques from CPP experiments [25,35]. One possibility is using a SQUID current amplifier, possibly combined with a cryogenic current comparator, which would have high sensitivity but requires inserting an inductor in the CPP loops [27]. A more detailed error analysis, including the impact of the biasing and measurement scheme, as well as consideration of niobium Josephson junctions for larger pump currents, is needed for a complete evaluation of the circuit for a possible resistance standard.

While the Josephson quantized Hall conductance device is unlikely to compete with existing metrological resistance standards, establishing experimentally that it quantizes transconductance is of immediate interest. The first step would be to verify the degeneracy structure with microwave spectroscopy in a superconducting circuit QED geometry and obtain an experimental equivalent of Fig. 5. Such spectroscopy measurements have been performed for superconducting qubits with drive-induced topology [36–38]. It may be possible to directly measure the local topological properties with such experiments [39–41]. If direct measurement of the transconductance encounters problems due to noise from the biasing circuit, techniques which avoid DC connections may be possible [42]. On the other hand, one could keep the DC connections and use microwave pumps to synchronize the DC voltages V_L and V_R, significantly reducing noise.

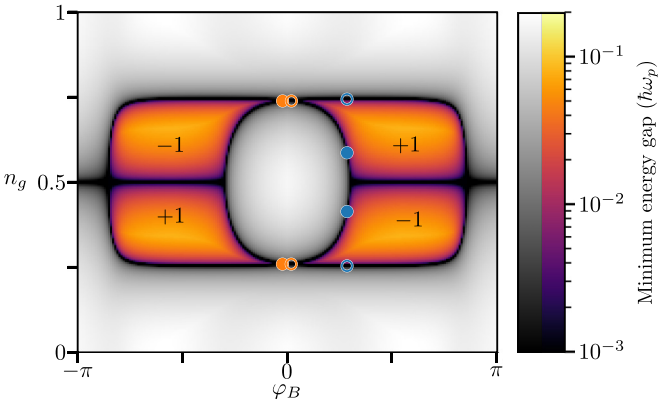

FIG. 5. Optimizing external parameters of the Josephson quantized Hall conductance device. The minimum energy gap for the symmetric Josephson quantized Hall conductance device is plotted as a function of global charge offset n_g and loop flux φ_B. Energies are scaled to the plasma frequency $\hbar\omega_p$, with a lower cutoff at 10^{-3}, and determined by minimizing the energy gap as a function of φ_L, φ_R for each value of n_g and φ_B. The topological charge of degeneracies is indicated by filled $(+1)$ and unfilled (-1) circles and correspond to the degeneracies in Figs. 4(b)–4(d). The Chern number $C(n_g, \varphi_B) = \pm 1$ is indicated in four topologically nontrivial regions delineated by black lines where the gap vanishes. Elsewhere, the system is topologically trivial (zero Chern number, gray regions). Fixing n_g and φ_B to have a large energy gap in a topologically nontrivial region results in transconductance quantization with minimal error due to nonadiabatic transitions.

We have observed that a circuit with an additional Josephson junction, giving it tetrahedral symmetry, also quantizes transconductance. This *tetrahedron* was considered previously as a candidate for a protected qubit [43]. It also has a rich topological structure and is part of the class of Weyl Josephson circuits [31]. From heuristic arguments and numerical calculations we conjecture that Josephson circuits with fewer than five tunnel junctions cannot quantize transconductance. However, such circuits may still display topologically nontrivial phenomena in their spectra, including the possibility of merging Dirac points [44–46]. Another variant five-junction circuit is the dual of the JHD [Fig. 7], a diamond-shaped circuit with three charge nodes and two loops which may also quantize transconductance.

Many other theoretical questions remain including a rigorous validation of the simultaneous fluxoid-charge pumping mechanism, determining the precise relationship between transconductance in JHD and the Andreev multiterminal systems, and computing additional topological invariants [47–50]. Establishing the theoretical optimum values for parameters such as α so as to maximize the energy gap and minimize errors is necessary and implies a deeper understanding of the behavior of the phase diagram [Fig. 5]. Investigating the topological properties of arbitrary Josephson Hamiltonians [31] may lead to their general classification and open possibilities for novel applications of quantum circuits. Our work shows that Josephson tunnel junctions are universal in

the sense that they can connect the three sides of the quantum metrology triangle relating f, V, and I. A major question remains as to whether such circuits can exhibit topological effects which go beyond this triangle.

ACKNOWLEDGMENTS

We thank V. Fatemi, L. Bretheau, and A. Akhmerov for insightful comments and corrections. We also thank J. Meyer, B. Douçot, D. Estève, H. Pothier, and F. Lafont for a critical reading of our manuscript. We acknowledge support from Jeunes Equipes de l'Institut de Physique du Collège de France. This research was supported by IDEX Grant No. ANR-10-IDEX-0001-02 PSL and a Paris "Programme Emergence(s)" Grant. This project has received funding from the European Research Council (ERC) under the European Union's Horizon 2020 research and innovation programme (Grant Agreement No. 636744).

APPENDIX

The Hamiltonian $H_J + H_C$ for the symmetric JHD circuit of the main text, reproduced in Fig. 6 with all parameters identified, is

$$\begin{aligned} H_J = & -E_{J1}\cos\hat{\delta}_1 - E_{J2}\cos\hat{\delta}_2 - E_{J3}\cos(\hat{\delta}_2 - \hat{\delta}_1 - \varphi_B) \\ & - E_{J4}\cos(\hat{\delta}_1 - \varphi_L) - E_{J5}\cos(\hat{\delta}_2 + \varphi_R), \\ H_C = & \, 2e^2(\hat{\mathbf{n}} - \mathbf{n_g})^T C^{-1}(\hat{\mathbf{n}} - \mathbf{n_g}), \end{aligned}$$

where the charge operators are $\hat{\mathbf{n}} = (\hat{n}_1, \hat{n}_2)$, the charge offsets are $\mathbf{n_g} = (n_{g1}, n_{g2})$, and the capacitance matrix C is given by

$$C = \begin{pmatrix} C_{J1} + C_{J3} + C_{J4} & -C_{J3} \\ -C_{J3} & C_{J2} + C_{J3} + C_{J5} \end{pmatrix}.$$

The gate capacitances, in general small compared to C_{Ji}, are neglected in C. The individual charging energies are $E_{Ci} = 2e^2/C_{Ji}$.

The Chern number associated to a two-dimensional (2D) plane spanning parameters X and Y can be computed from the Berry curvature of the ground state $|\psi\rangle$:

$$B_{X,Y} = -2\,\mathrm{Im}\left\langle \frac{\partial\psi}{\partial X} \middle| \frac{\partial\psi}{\partial Y} \right\rangle.$$

For a φ_L, φ_R sweep and a given set of equal charge offsets n_g and reduced flux φ_B, we define the Chern number as the integral of B_{φ_R,φ_L} over the whole φ_L, φ_R plane:

$$C(n_g, \varphi_B) = \frac{1}{2\pi}\int_0^{2\pi}\int_0^{2\pi} d\varphi_L d\varphi_R B_{\varphi_R,\varphi_L}.$$

Following [14,30] we obtain Eq. (1), where we have a plus sign for both I_L and I_R since positive voltage V_R corresponds to negative $\dot{\varphi}_R$ given the circuit conventions of Fig. 6.

For numerical calculations, circuit Hamiltonians are directly written in the charge basis with typically 10 charge states for each island. Eigenvalues and eigenstates are obtained by direct diagonalization of the sparse Hamiltonian matrix via the Lanczos algorithm as implemented in SCIPY [51]. To determine the Berry curvature, the gradient of the Hamiltonian with respect to external parameters is calculated analytically and then converted to the charge basis. Chern numbers are obtained by numerical integration of the Berry curvature over the desired 2D surface in parameter space. The precise locations of degeneracies are obtained with minimization techniques such as simplicial homology global optimization in SCIPY [52]. Parameters used to obtain the spectra and degeneracies in Fig. 4 are $E_{J1} = 1.0$, $E_{J2} = 0.8$, $E_{J3} = 1.1$, $E_{J4} = 0.9$, $E_{J5} = 1.2$ and we keep the plasma energy constant $\hbar\omega_p = \sqrt{2E_{Ji}E_{Ci}} = 1$ such that $E_{Ci} = 1/E_{Ji}$. This corresponds to the experimentally relevant situation where the surface area of the Josephson junctions may be different, but since the oxidation process for the tunnel barriers is common, the plasma frequencies are the same.

For the spectra of Fig. 4(b) the cuts are made in the φ_L, φ_R plane at fixed ϕ_B, n_g along the diagonals shown in the bottom planes of Figs. 4(c) and 4(d) and given by the following equations:

$$\varphi_R = 0.7195\varphi_L + 0.8811 \ (\varphi_B = 0, n_g = 0.2598, \text{orange}),$$
$$\varphi_R = 0.7195\varphi_L + 0.7092 \ (\varphi_B = 0.9, n_g = 0.2541, \text{blue}).$$

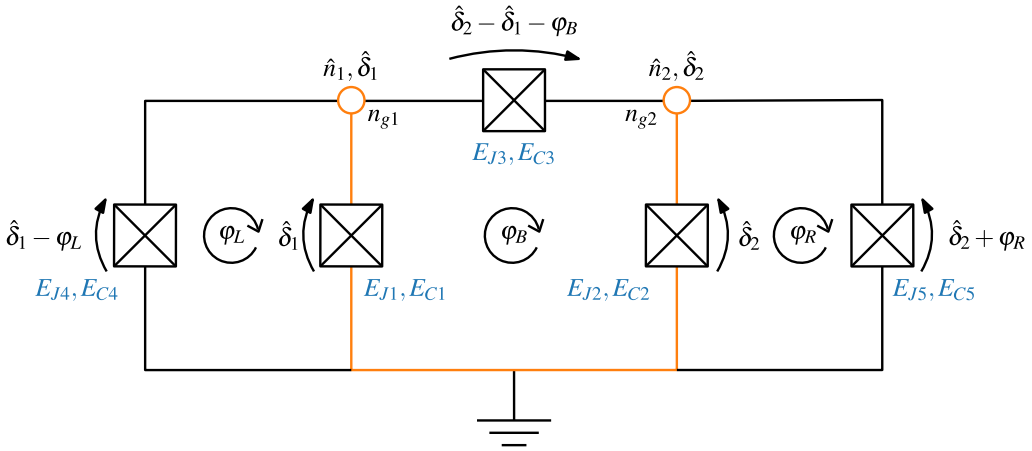

FIG. 6. Full circuit of symmetric Josephson quantized Hall conductance device.

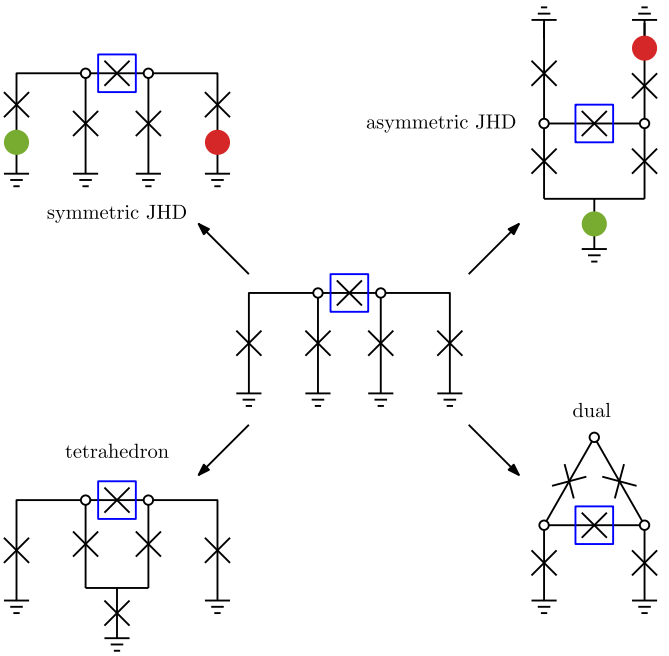

FIG. 7. Correspondence between the symmetric and asymmetric Josephson quantized Hall conductance devices, the dual JHD circuit, and the tetrahedron circuit. The elementary five-junction JHD circuit shown in Fig. 1 (center) can be mapped to the circuit of Fig. 4 (upper left) by adding voltage sources (red and green circles). To obtain the circuit of Fig. 3, the green source is inserted as shown in the upper right and the remaining circuit is folded upward. The tetrahedron circuit (lower left) requires an additional junction. The JHD dual circuit (lower right) is constructed from the dual graph of the central circuit after connecting grounds. Whereas the JHD has two islands (unfilled circles) and three loops, the dual circuit has three islands and two loops. Although transconductance is quantized in the JHD and tetrahedron, we have not verified that this is true for the dual JHD circuit.

The positions and topological charges of degeneracies in Figs. 4(c) and 4(d) are given in Table I. The source code is available on Zenodo [53].

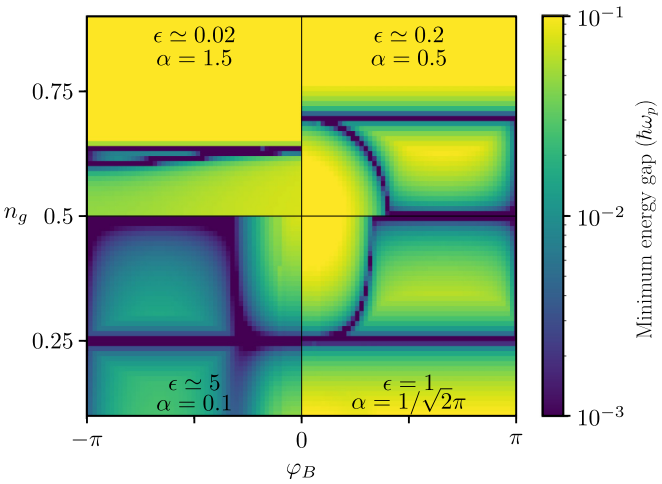

FIG. 8. Optimizing internal parameters of the Josephson quantized Hall conductance device. The minimum energy gap diagram of Fig. 5 is reproduced for identical junctions and with each quadrant corresponding to a different value of the normalized junction impedance $\alpha = Z_J/R_Q = 1/2\pi\sqrt{2E_C/E_J}$ or energy ratio $\epsilon = E_J/E_C$. For a given value of α, the quadrants not shown are related by symmetry. Energy is plotted in units of the plasma frequency $\hbar\omega_p = \sqrt{2E_JE_C}$ which is constant so that the gap can be compared for different values of α, and gap values beyond the color scale are capped. The upper left corresponds to the deep charging regime $E_C \gg E_J$ and the Chern number is zero everywhere except in the top left pocket. The degeneracies are located almost entirely on the horizontal line at $n_g \approx \frac{5}{8}$ (and $n_g \approx \frac{3}{8}$ by symmetry) as expected for a Cooper pair pump in which the exterior capacitances are doubled. As the Josephson energy is increased clockwise, the topologically nontrivial region grows out from the corner pockets where these horizontal lines reach $\varphi_B = \pm\pi$. An additional horizontal degeneracy line appears at $n_g = \frac{1}{2}$ and the ones at $n_g = \frac{2}{3}$ ($n_g = \frac{1}{3}$) move out toward $n_g = \frac{3}{4}$ ($n_g = \frac{1}{4}$). From the color scale, the minimum energy gap is maximized near $\alpha = 0.5$ (upper right). By designing the junction area $S \propto 1/\alpha$ for the optimal impedance, the energy gap in the topologically nontrivial region is maximized, reducing error in transconductance quantization due to Landau-Zener transitions. The bottom right quadrant ($\epsilon = 1$) can be compared to Fig. 5, where the junctions are not identical but the average E_{Ji}/E_{Ci} is approximately one. As junction uniformity is reduced, the corners of the nontrivial region are pulled back.

TABLE I. Positions in parameter space φ_L, φ_R, n_g and topological charges χ of degeneracies in Fig. 4.

Fig. 4(c) $\varphi_B = 0$				Fig. 4(d) $\varphi_B = 0.9$			
φ_L	φ_R	n_g	χ	φ_L	φ_R	n_g	χ
3.7806	3.6014	0.2598	−1	3.5632	3.2152	0.2541	−1
2.5026	2.6818	0.2598	+1	1.9204	2.0659	0.4211	+1
2.5026	2.6818	0.7403	+1	1.9204	2.0659	0.5789	+1
3.7806	3.6014	0.7403	−1	3.5632	3.2152	0.7459	−1

[1] M. Kjaergaard, M. E. Schwartz, J. Braumüller, P. Krantz, J. I.-J. Wang, S. Gustavsson, and W. D. Oliver, Superconducting qubits: Current state of play, Annu. Rev. Condens. Matter Phys. **11**, 369 (2020).

[2] M. Buchner, K. Höfler, B. Henne, V. Ney, and A. Ney, Tutorial: Basic principles, limits of detection, and pitfalls of highly sensitive squid magnetometry for nanomagnetism and spintronics, J. Appl. Phys. **124**, 161101 (2018).

[3] R. L. Kautz, Noise, chaos, and the Josephson voltage standard, Rep. Prog. Phys. **59**, 935 (1996).

[4] A. Rüfenacht, N. E. Flowers-Jacobs, and S. P. Benz, Impact of the latest generation of Josephson voltage standards in ac and dc electric metrology, Metrologia **55**, S152 (2018).

[5] J. P. Pekola, O.-P. Saira, V. F. Maisi, A. Kemppinen, M. Mottonen, Y. A. Pashkin, and D. V. Averin, Single-electron current sources: Towards a refined definition of ampere, Rev. Mod. Phys. **85**, 1421 (2013).

[6] N.-H. Kaneko, S. Nakamura, and Y. Okazaki, A review of the quantum current standard, Meas. Sci. Technol. **27**, 032001 (2016).

[7] W. Poirier, S. Djordjevic, F. Schopfer, and O. Thévenot, The ampere and the electrical units in the quantum era, C. R. Phys. **20**, 92 (2019).

[8] W. Poirier, F. Schopfer, J. Guignard, O. Thévenot, and P. Gournay, Application of the quantum Hall effect to resistance metrology, C. R. Phys. **12**, 347 (2011).

[9] R. Ribeiro-Palau, F. Lafont, J. Brun-Picard, D. Kazazis, A. Michon, F. Cheynis, O. Couturaud, C. Consejo, B. Jouault, W. Poirier, and F. Schopfer, Quantum Hall resistance standard in graphene devices under relaxed experimental conditions, Nat. Nanotechnol. **10**, 965 (2015).

[10] A. M. Hriscu and Y. V. Nazarov, Quantum Synchronization of Conjugated Variables in a Superconducting Device Leads to the Fundamental Resistance Quantization, Phys. Rev. Lett. **110**, 097002 (2013).

[11] B. van Heck, S. Mi, and A. R. Akhmerov, Single fermion manipulation via superconducting phase differences in multi-terminal Josephson junctions, Phys. Rev. B **90**, 155450 (2014).

[12] T. Yokoyama and Y. V. Nazarov, Singularities of Andreev spectrum in multi-terminal Josephson junction, Phys. Rev. B **92**, 155437 (2015).

[13] H.-Y. Xie, M. G. Vavilov, and A. Levchenko, Topological Andreev bands in three-terminal Josephson junctions, Phys. Rev. B **96**, 161406(R) (2017).

[14] R.-P. Riwar, M. Houzet, J. S. Meyer, and Y. V. Nazarov, Multi-terminal Josephson junctions as topological matter, Nat. Commun. **7**, 11167 (2017).

[15] E. Eriksson, R.-P. Riwar, M. Houzet, J. S. Meyer, and Y. V. Nazarov, Topological transconductance quantization in a four-terminal Josephson junction, Phys. Rev. B **95**, 075417 (2017).

[16] J. S. Meyer and M. Houzet, Non-Trivial Chern Numbers in Three-Terminal Josephson Junctions, Phys. Rev. Lett. **119**, 136807 (2017).

[17] H.-Y. Xie, M. G. Vavilov, and A. Levchenko, Weyl nodes in Andreev spectra of multiterminal Josephson junctions: Chern numbers, conductances, and supercurrents, Phys. Rev. B **97**, 035443 (2018).

[18] A. W. Draelos, M.-T. Wei, A. Seredinski, H. Li, Y. Mehta, K. Watanabe, T. Taniguchi, I. V. Borzenets, F. Amet, and G. Finkelstein, Supercurrent flow in multiterminal graphene Josephson junctions, Nano Lett. **19**, 1039 (2019).

[19] G. V. Graziano, J. S. Lee, M. Pendharkar, C. J. Palmstrøm, and V. S. Pribiag, Transport studies in a gate-tunable three-terminal Josephson junction, Phys. Rev. B **101**, 054510 (2020).

[20] N. Pankratova, H. Lee, R. Kuzmin, K. Wickramasinghe, W. Mayer, J. Yuan, M. G. Vavilov, J. Shabani, and V. E. Manucharyan, Multiterminal Josephson Effect, Phys. Rev. X **10**, 031051 (2020).

[21] D. J. Thouless, Topological quantum numbers in nonrelativistic physics, Int. J. Mod. Phys. B **11**, 3319 (1997).

[22] D. J. Thouless, *Topological Quantum Numbers in Nonrelativistic Physics* (World Scientific, Singapore, 1998).

[23] R. Leone and L. Lévy, Topological quantization by controlled paths: Application to cooper pairs pumps, Phys. Rev. B **77**, 064524 (2008).

[24] L. J. Geerligs, S. M. Verbrugh, P. Hadley, J. E. Mooij, H. Pothier, P. Lafarge, C. Urbina, D. Estève, and M. H. Devoret, Single cooper pair pump, Z. Phys. B **85**, 349 (1991).

[25] P. A. Erdman, F. Taddei, J. T. Peltonen, R. Fazio, and J. P. Pekola, Fast and accurate cooper pair pump, Phys. Rev. B **100**, 235428 (2019).

[26] R. Léone, L. P. Lévy, and P. Lafarge, The Cooper Pair Pump as a Quantized Current Source, Phys. Rev. Lett. **100**, 117001 (2008).

[27] J. Brun-Picard, S. Djordjevic, D. Leprat, F. Schopfer, and W. Poirier, Practical Quantum Realization of the Ampere from the Elementary Charge, Phys. Rev. X **6**, 041051 (2016).

[28] I. Zapata, R. Bartussek, F. Sols, and P. Hänggi, Voltage Rectification by a Squid Ratchet, Phys. Rev. Lett. **77**, 2292 (1996).

[29] A. Sterck, R. Kleiner, and D. Koelle, Three-Junction Squid Rocking Ratchet, Phys. Rev. Lett. **95**, 177006 (2005).

[30] V. Gritsev and A. Polkovnikov, Dynamical quantum Hall effect in the parameter space, Proc. Natl. Acad. Sci. USA **109**, 6457 (2012).

[31] V. Fatemi, A. R. Akhmerov, and L. Bretheau, Weyl Josephson circuits, Phys. Rev. Research **3**, 013288 (2021).

[32] D. Guéry-Odelin, A. Ruschhaupt, A. Kiely, E. Torrontegui, S. Martínez-Garaot, and J. G. Muga, Shortcuts to adiabaticity: Concepts, methods, and applications, Rev. Mod. Phys. **91**, 045001 (2019).

[33] J. J. Vartiainen, M. Mottonen, J. Pekola, and A. Kemppinen, Nanoampere pumping of Cooper pairs, Appl. Phys. Lett. **90**, 082102 (2007).

[34] M. Aunola and J. J. Toppari, Connecting berry's phase and the pumped charge in a cooper pair pump, Phys. Rev. B **68**, 020502(R) (2003).

[35] M. Mottonen, J. J. Vartiainen, and J. P. Pekola, Experimental Determination of the Berry Phase in a Superconducting Charge Pump, Phys. Rev. Lett. **100**, 177201 (2008).

[36] P. J. Leek, J. M. Fink, A. Blais, R. Bianchetti, M. Goppl, J. M. Gambetta, D. I. Schuster, L. Frunzio, R. J. Schoelkopf, and A. Wallraff, Observation of Berry's phase in a solid-state qubit, Science **318**, 1889 (2007).

[37] P. Roushan, C. Neill, Y. Chen, M. Kolodrubetz, C. Quintana, N. Leung, M. Fang, R. Barends, B. Campbell, Z. Chen, B. Chiaro, A. Dunsworth, E. Jeffrey, J. Kelly, A. Megrant, J. Mutus, P. J. J. O'Malley, D. Sank, A. Vainsencher, J. Wenner *et al.*, Observa-

tion of topological transitions in interacting quantum circuits, Nature (London) **515**, 241 (2014).

[38] M. D. Schroer, M. H. Kolodrubetz, W. F. Kindel, M. Sandberg, J. Gao, M. R. Vissers, D. P. Pappas, A. Polkovnikov, and K. W. Lehnert, Measuring a Topological Transition in an Artificial Spin-1/2 System, Phys. Rev. Lett. **113**, 050402 (2014).

[39] T. Ozawa and N. Goldman, Extracting the quantum metric tensor through periodic driving, Phys. Rev. B **97**, 201117(R) (2018).

[40] R. L. Klees, G. Rastelli, J. C. Cuevas, and W. Belzig, Microwave Spectroscopy Reveals the Quantum Geometric Tensor of Topological Josephson Matter, Phys. Rev. Lett. **124**, 197002 (2020).

[41] X. Tan, D.-W. Zhang, Z. Yang, J. Chu, Y.-Q. Zhu, D. Li, X. Yang, S. Song, Z. Han, Z. Li, Y. Dong, H.-F. Yu, H. Yan, S.-L. Zhu, and Y. Yu, Experimental Measurement of the Quantum Metric Tensor and Related Topological Phase Transition with a Superconducting Qubit, Phys. Rev. Lett. **122**, 210401 (2019).

[42] F. Nguyen, N. Boulant, G. Ithier, P. Bertet, H. Pothier, D. Vion, and D. Esteve, Current to Frequency Conversion in a Josephson Circuit, Phys. Rev. Lett. **99**, 187005 (2007).

[43] M. V. Feigel'man, L. B. Ioffe, V. B. Geshkenbein, P. Dayal, and G. Blatter, Superconducting Tetrahedral Quantum Bits, Phys. Rev. Lett. **92**, 098301 (2004).

[44] A. Monjou and R. Leone, Merging diabolical points of a superconducting circuit, Condens. Matter Phys. **16**, 33801 (2013).

[45] X. Tan, Y. Zhao, Q. Liu, G. Xue, H. Yu, Z. D. Wang, and Y. Yu, Realizing and manipulating space-time inversion symmetric topological semimetal bands with superconducting quantum circuits, npj Quantum Mater. **2**, 1 (2017).

[46] X. Tan, D.-W. Zhang, Q. Liu, G. Xue, H.-F. Yu, Y.-Q. Zhu, H. Yan, S.-L. Zhu, and Y. Yu, Topological Maxwell Metal Bands in a Superconducting Qutrit, Phys. Rev. Lett. **120**, 130503 (2018).

[47] S.-C. Zhang and J. Hu, A Four-Dimensional Generalization of the Quantum Hall Effect, Science **294**, 823 (2001).

[48] F. Zhang and C. L. Kane, Anomalous topological pumps and fractional Josephson effects, Phys. Rev. B **90**, 020501(R) (2014).

[49] G. Palumbo and N. Goldman, Tensor Berry connections and their topological invariants, Phys. Rev. B **99**, 045154 (2019).

[50] X. Tan, D.-W. Zhang, D. Li, X. Yang, S. Song, Z. Han, Y. Dong, D. Lan, H. Yan, S.-L. Zhu, and Y. Yu, Experimental Observation of Tensor Monopoles with a Superconducting Qudit, Phys. Rev. Lett. **126**, 017702 (2021).

[51] https://www.scipy.org/.

[52] https://docs.scipy.org/doc/scipy/reference/generated/scipy.optimize.shgo.html.

[53] L. Peyruchat, J. Griesmar, J.-D. Pillet, and Ç. Ö. Girit, FluxQuantumLab/JHD-paper-zenodo, 10.5281/zenodo.4048048.